How additives affect Cu electrodeposition : an electrochemical STM Study

Yanson, Y.I.

Chapter 1

Background

This chapter contains basic background knowledge of concepts, theories, and experimental techniques, relevant for the matter of this thesis. The process of electrodeposition is described, followed by a more detailed explanation of different mechanisms of deposition. The experimental techniques that are described in this chapter include cyclic voltammetry, chronoamperometry, infrared and Raman spectroscopy, and scanning tunneling microscopy with an emphasis on its application in an electrochemical environment.

1.1 Electrodeposition

Electrodeposition is a process of depositing a coating on a conducting (metal) substrate immersed in an ionic conducting electrolyte by the application of electric current. The electrolyte generally consists of the electroactive species to be deposited and a supporting electrolyte to improve its conductivity. The electrodeposition process, known for more than 150 years, is nowadays widely used by the industry as it offers various advantages compared to other deposition techniques. The advantages include its ease of use, its low cost, control over the deposited layer properties, scalability etc. The typical applications of electrodeposition include deposition of layers on surfaces for improvement of corrosion and wear resistance, of decoration purposes, and of thermal and electrical conductivity. The unique property of electrodeposition is that it allows to produce coatings with regular and non-porous structures even on complex shapes.

Copper was the first metal ever to be electrodeposited, as it was used to plate printing press plates as early as in 1839. Thus, a vast body of knowledge exists concerning Cu electrodeposition on various surfaces. However, the process of Cu deposition is far from being completely understood. Nowadays, one of the major applications of Cu electrodeposition is the deposition of interconnects on semiconductor integrated circuits, called chips, as it forms a very important step in the chip manufacturing. Due to the trend of miniaturization of the electronics, the industry faces a major challenge as smaller and smaller features, the so-called vias, need to be filled with Cu without forming any defects, such as voids, that could impair the operation of the chip. Figure 1.1a shows an SEM image of a cross section of a via, filled with Cu by electrodeposition, that has a void. To fill the vias completely without forming any voids, various substances are added to the electroplating baths. These substances are called additives. The process of void-less filling is called bottom-up superfilling, see Fig. 1.1b.

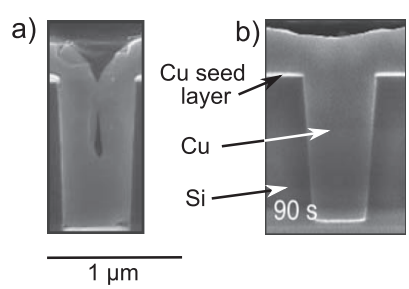

Figure 1.1: SEM images of via cross sections. Vias were electrochemically filled with copper. a) A void has formed in the via. b) A via that was filled bottom-up (superfilling) from a solution containing special additives. The images are reproduced with permission from [1].

Via filling with copper is only one example out of a great multitude of processes,

where additives play a crucial role for obtaining deposits of desired properties [2]. For most of the processes, the precise composition of the electrolyte is tuned by trial and error. Therefore, the understanding of the action of each of the additives of the plating electrolyte is usually missing.

1.2 Electrochemical interfaces

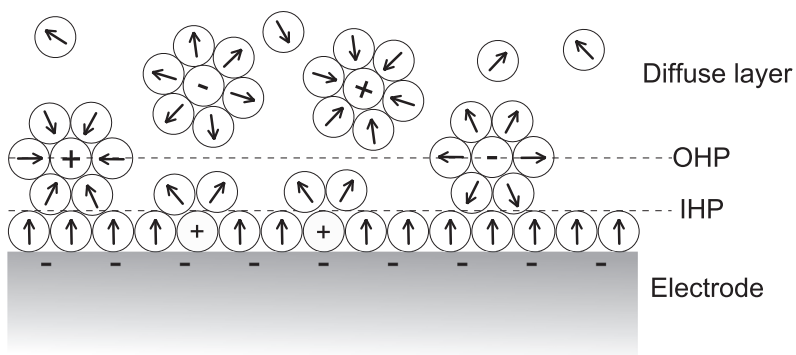

Figure 1.2: Schematic representation of the double-layer structure in an electrolyte solution close to the interface with an electrode. Specifically adsorbed ions are located in the inner Helmholtz plane (IHP), whereas solvated non-specifically adsorbed ions are found in the outer Helmholtz plane (OHP). The specifically adsorbed ions may transfer a part of their charge or their complete charge to the electrode [3].

At the interface between an electrode and an electrolyte, the so-called electrical double-layer is formed. In general, it is defined as a layer at the interface at which a variation of electric potential is present. This variation is not large ($\sim$ 1 V), but due to a small width of the double-layer, electric fields of significant strength (10^8 V cm^{-1}) develop at the interface. This large field at an electrode/electrolyte interface is, in a sense, the essence of electrochemistry in general and electrochemical deposition in particular. A model of the electrical double-layer is shown in Fig. 1.2. Several layers can be distinguished in the double-layer. The layer that is the closest to the electrode is called the inner Helmholtz plane (IHP). In this layer, the dipoles of the polar solvent (water) molecules feel the charge (negative or positive) of the electrode and tend to arrange themselves in a preferred orientation, forming the so-called hydration sheath. The ions that are present in the IHP form strong chemical bonds with the electrode surface. These ions are said to be specifically adsorbed, i.e. with at least a component deriving from a direct chemical interaction. Somewhat further away from the electrode, the outer Helmholtz plane (OHP) is located. The ions in this plane keep their hydration

shells (at least partly) and interact only weakly with the electrode via electrostatic forces. These ions are said to be non-specifically adsorbed. The rest of the double-layer region, containing solvated ions and solvent molecules, is called the diffuse layer.

In this section we will focus on several phenomena found at an electrode/electrolyte interface, such as the adsorption of thiol molecules, metal underpotential deposition (UPD), and metal bulk deposition, that are relevant for this thesis. For general information on electrode/electrolyte interfaces, the reader is referred to [3, 4].

1.2.1 Thiol adsorption on metals

Thiols are organic molecule that consist of an *–SH* head group, an organic (alkane) spacer, and a functional tail group. Thiols are known to adsorb very strongly on metal surfaces due to the formation of a strong covalent bond (bond strength of up to 200 $\mathrm{kJ\,mole^{-1}}$ on Au [5]) of the sulfur head group to metals. It has been found that upon adsorption on (coinage) metal surfaces, thiols tend to spontaneously arrange themselves in well-ordered monolayers, the so-called self-assembled monolayers (SAMs).

The strong thiol-metal bond leads to a wide potential window, in which the thiol SAMs are stable. For example, desorption of thiols from a gold electrode can occur either via reductive desorption at more negative potentials, where it often overlaps with the hydrogen evolution reaction, or via oxidative desorption at more positive potentials, which, in the case of a gold electrode, overlaps with the gold oxidation reaction.

Gold, in general, has been the substrate of choice for various reasons not only in electrochemical but also in the countless other studies of thiol-based SAMs. Especially the SAMs on (111)-oriented Au electrodes (single crystals or films deposited on mica or quartz) have been studied the most. Recent experiments have provided indirect and direct evidence that the gold surface undergoes significant restructuring upon SAM formation; the gold adatoms are either located in between two thiolate species [6] or are found as part of a gold thiolate species, in between the molecule and the Au surface [7].

Amongst the numerous potential applications of thiols, especially in the SAM form, such as corrosion inhibition, surface patterning, electroanalysis etc., we would like to point out the use of thiols as additives for electrodeposition. Thiols, depending on their exact structure, can influence the electrodeposition process and the resulting deposit in various, sometimes even opposite ways. For Cu interconnect metallization, bis(3-sulfopropyl)disulfide (SPS) or its monomer, 3-mercapto-1-propanesulfonic (MPS), is used as brightener and as accelerator [2]. The use of these substances in plating solutions to promote the bottom-up fill was empirically developed by IBM in 1998 [2]. However, despite the tremendous importance of the process, the exact role of SPS (MPS) still remains controversial.

1.2.2 Metal overpotential deposition

Overpotential deposition or bulk deposition of a metal M occurs at an electrode surface S at potentials negative with respect to the equilibrium (Nernst) potential E_{eq} of the $M^{z+} + ze^- \rightleftarrows M$ reaction (in some systems underpotential deposition may occur, see further in the text). At potentials positive with respect to the Nernst potential, the metal M becomes unstable and dissolves anodically. At the Nernst equilibrium potential no net deposition or dissolution occur. The negative departure of the electrode potential from its equilibrium potential is called overpotential.

The deposition overpotential η is directly linked to the supersaturation $\triangle\mu$ of the M atoms at the electrode surface. The two are related in the electrochemical environment by the following relation [8]:

$$\triangle\mu = ze\eta. \tag{1.1}$$

Thus, if one would conduct electrodeposition at a constant overpotential, i.e. under potentiostatic control, it would lead to a constant supersaturation at the electrode surface. In the industrial environment, however, electrodeposition is mostly carried out at constant deposition current, i.e. under galvanostatic control.

Three stages of metal electrodeposition can be distinguished:

1. Mass transfer, i.e. transport of metal ions from the bulk of the solution towards the electrode surface via diffusion and convection.

2. Charge transfer, i.e. transition of the double-layer by the metal ions, accompanied by the removal of the solvation shells of the ions, adsorption of the ions at the electrode, and the electron transfer reaction to convert the ions into neutral metal atoms.

3. Crystallization of the new phase, which proceeds via nucleation and growth.

In the following we will describe each of these stages in more details. Additionally, we will discuss the rules that define the shape of the crystallites.

1.2.2.1 Mass transfer

The supply of metal ions to the electrode surface proceeds via diffusion, convection, or electric migration. The electric migration of the metal ions, which occurs due to the influence of an electric field on the ions in the bulk of the electrolyte, is usually suppressed by the presence of the so-called supporting electrolyte with a much higher ionic concentration than that of the metal ions. In such conditions electric migration can be neglected, since the overall current through the solution is transferred by the supporting electrolyte.

Convection plays a very important role in industrial metal deposition as it allows to achieve larger deposition currents, and thus higher deposition speeds, by enhancing

the supply of ions to the electrode surface. In laboratory environments, rotating disk electrode (RDE) setups are used to maintain a steady convective flux towards the electrode. Here, we will describe mass transfer via diffusion only, as this is the only relevant mechanism with respect to the experiments presented in this thesis.

If the transport process in the electrolyte consists purely of diffusion, then the flux is given by Fick's first law:

$$j = -D\frac{\partial C}{\partial x}, \tag{1.2}$$

where D is the diffusion constant and C is the concentration of the ions in the solution and x is the spacial coordinate perpendicular to the surface. We would like to note that the one-dimensional form of Fick's first law, as given by Eq. 1.2, is true for an infinitely large planar electrode. In general, for an electrode of a finite size the three-dimensional form of Eq. 1.2 has to be considered. In practice, the influence of the finite electrode size can be neglected for the disc electrodes with a diameter of a few millimeters. To obtain the flux towards the electrode surface, the concentration gradient at $x = 0$ has to be considered. On the other hand, concentration is a function of time during electrodeposition, as the ions are constantly consumed at the electrode surface. To obtain the space and time variation of the concentration, it is necessary to solve Fick's second law under appropriate initial boundary conditions:

$$\frac{\partial C}{\partial t} = D\frac{\partial^2 C}{\partial x^2}. \tag{1.3}$$

In the following, we will derive equations for the electrochemical deposition current for two cases: one for a planar electrode and one for a growing hemispherical nucleus, under the assumption that the diffusion is the rate-limiting step of the electrodeposition process. In the case of a planar electrode, Eq. 1.3 has to be solved with the following boundary conditions:

$$\begin{aligned} C(x,0) &= C_b \\ \lim_{x\to\infty} C(x,t) &= C_b \\ C(0,t) &= 0 \end{aligned} \tag{1.4}$$

Here C_b is the concentration in the bulk of the solution. The last boundary condition in 1.4 means that all the ions that get in contact with the electrode surface are instantaneously reduced into neutral atoms. In this case one refers to the process as being diffusion-limited. The solution of Fick's second law under these boundary conditions is:

$$C(x,t) = C_b \operatorname{erf}\left(\frac{x}{\sqrt{4Dt}}\right). \tag{1.5}$$

Substituting Eq. 1.5 into Eq. 1.2 and taking into account the Faraday law of electrolysis[1], we obtain the following relationship for the electrochemical current density $i(t)$, which is known as the Cottrell equation:

$$i(t) = \frac{zF\sqrt{D}C_b}{\sqrt{\pi t}}, \tag{1.6}$$

where F is the Faraday constant and z is the charge of the ions in signed units of electronic charge. Please note that we switch from the flux of the ions in Eq. 1.2 to the current density in Eq. 1.6, since it is the electrical current that is usually measured in the electrochemical experiments. Although the Cottrell equation has been developed for a simple redox reaction at a stationary non-changing electrode, it can be also used to describe the electrochemical current due to electrodeposition of material onto an electrode. In principle, the Cottrell equation would describe the time-dependence of the diffusion-limited electrochemical deposition current in the case, where no (3D) nucleation is necessary to grow the electrodeposited material. This would be the case for deposition of material onto an electrode of the same material containing a large amount of special defects, the so-called kink sites. In practice, the electrochemical current of metal deposition is found to follow the Cottrell current at sufficiently long deposition times, i.e. after the diffusion zones around individual nuclei have grown into full overlap with each other.

In the case of the diffusion to a hemispherical nucleus of radius r_n, Fick's second law has to be rewritten in spherical coordinates

$$\frac{\partial C}{\partial t} = D\left(\frac{\partial^2 C}{\partial r^2} + \frac{2}{r}\frac{\partial C}{\partial r}\right) \tag{1.7}$$

and solved with the following boundary conditions:

$$\begin{aligned} C(r,0) &= C_b\,,\ r \geq r_n \\ \lim_{r\to\infty} C(r,t) &= C_b \\ C(r_n,t) &= 0 \end{aligned} \tag{1.8}$$

This problem is solved by:

$$C(r,t) = C_b\left(1 - \frac{r_n}{r}\,\mathrm{erfc}\left[\frac{r-r_n}{\sqrt{4Dt}}\right]\right). \tag{1.9}$$

Thus, the flux of the ions to the nucleus surface is

$$j(t) = DC_b\left(\frac{1}{\sqrt{D\pi t}} + \frac{1}{r_n}\right). \tag{1.10}$$

[1] The Faraday law of electrolysis states that the amount of substance produced at an electrode is proportional to the current that is passed through it.

The current[1] at the hemispherical nucleus is then given by

$$I(t) = zF2\pi r_n DC_b. \tag{1.11}$$

On the other hand, the current of a growing hemispherical nucleus can be written as:

$$I(t) = zFV_m\frac{\mathrm{d}V}{\mathrm{d}t} = zFV_m 2\pi r_n^2\frac{\mathrm{d}r_n}{\mathrm{d}t}, \tag{1.12}$$

where V is the volume of the nucleus and V_m is the molar volume of the material. By combining Eqs. 1.11 and 1.12, one can calculate the time-dependence of the nucleus radius $r_n(t)$. Then, by substituting $r_n(t)$ in Eq. 1.11 the following expression for the current is obtained:

$$I(t) = zF\pi(2DC_b)^{3/2}V_m^{1/2}t^{1/2}. \tag{1.13}$$

Equation 1.13 is used in the derivation of various models describing the electrochemical current due to nucleation and growth under diffusion control. However, as one might suspect, it is not completely correct for the case of a growing nucleus, as we have assumed in Eq. 1.8 that the nucleus has a constant radius r_n. However, it has been shown that if growth of the nucleus is taken into account, i.e. a moving boundary is considered, the resulting current is virtually identical with the one given by Eq. 1.13 for reasonable values of C_b and V_m [9, 10].

1.2.2.2 Charge transfer

Charge transfer refers to the process, in which an ion crosses the double-layer region at the interface between the bulk electrolyte and the electrode, becoming a neutral atom at the surface. It is charge transfer that defines the electrochemical kinetics at the electrode. One of the most fundamental relationships that describe electrode kinetics is the Butler-Volmer equation [4]. It provides the dependence of the electrochemical current density at an electrode on its potential:

$$i = i_0\left(\exp\left[\frac{\alpha zF\eta}{RT}\right] - \exp\left[\frac{(1-\alpha)zF\eta}{RT}\right]\right). \tag{1.14}$$

Here η is the difference between the applied electrode potential and the equilibrium potential of the reaction, i_0 is the exchange current density and α is the charge transfer coefficient. The exchange current density defines the electrochemical current that flows at zero overpotential to the electrode due to the reduction of ions and from the electrode due to the oxidation of atoms, resulting in a zero net current. The charge transfer coefficient is a measure of the symmetry of the standard free energy barrier of the charge transfer reaction [4]; $\alpha = 0.5$ for a symmetrical barrier.

[1] Throughout this thesis the current density is denoted as i, whereas the total current (integrated over the entire surface) is denoted as I.

Equation 1.14 assumes that all z electrons are transferred in one step during a multi-electron transfer reaction. However, this is definitely not the case for most of the electrochemical reactions, as a simultaneous multi-electron transfer is highly improbable and the electrons are transferred in a series of one-electron steps [11]. Generally, a multi-step electrochemical reaction involves one or more fast steps and a slow step, which is called the rate-determining step. For example, it has has been shown that the overall reduction of copper ions $Cu^{2+} + 2e^- \rightarrow Cu$ in sulfuric acid supporting electrolyte proceeds via the following steps [12]:

$$\begin{aligned} Cu^{2+} + e^- &\rightarrow Cu^+ \ \text{slow} \\ Cu^+ + e^- &\rightarrow Cu \ \text{fast}, \end{aligned} \tag{1.15}$$

where the first step is the rate-determining step of the reaction.

Equation 1.14 can be modified to account for a reaction, in which z total electrons are transferred in z steps, with z_f fast steps preceding ν slow rate-determining steps and followed by $z - z_f - \nu$ fast steps [3, 13]:

$$i(t) = i_0 \left\{ \exp\left[\left(\frac{z_f}{\nu} + \alpha \right) \frac{F\eta}{RT} \right] - \exp\left[-\left(\frac{z - z_f}{\nu} - \alpha \right) \frac{F\eta}{RT} \right] \right\}. \tag{1.16}$$

To derive Eq. 1.16 it is assumed that for the forward reaction (first term in the brackets), such as the deposition, the concentration of the species that take part in the rate-determining steps is given by the z_f fast reaction steps. For the reverse reaction (second term in the brackets), such as the dissolution, the concentration of the species for the slow steps is obtained by performing $z - z_f - \nu$ fast reaction steps.

1.2.2.3 Nucleation and growth

Nucleation and growth of a new phase is a very broad subject that has been covered in various books not only for the case of electrochemical interfaces [8, 14, 15], but also for the phase formation in vacuum, melts, supersaturated solutions etc [16, 17]. Here we will focus only on several basic concepts that are relevant for the matter of this thesis.

In general, the formation of a nucleus on a substrate is not an instantaneous process. The reason for it is that there is a certain barrier in the Gibbs free energy associated with the formation of a cluster that consist of n atoms, the so-called nucleation work:

$$\triangle G(n) = -n \triangle \mu + \Phi(n). \tag{1.17}$$

If the formation of a 3D nucleus is considered, then $\Phi(n)$ corresponds to the surface free energy of the nucleus. An equation similar to Eq. 1.17 can be written for the case of 2D nucleus formation, in which $\Phi(n)$ would correspond to the step free energy of the nucleus. The first term in Eq. 1.17 is proportional to the number of atoms n, which

defines the volume of the nucleus in the 3D nucleation case and its surface area in the 2D case. The second term is proportional to the surface area of the 3D nucleus ($\sim n^{2/3}$), or to the perimeter of the 2D nucleus ($\sim n^{1/2}$). Thus, the nucleation work has a maximum, see Fig. 1.3. This maximum corresponds to the so-called critical nucleus size n_c. The nucleus of this size is in the unstable equilibrium phase with the solution and the attachment of more atoms would lead to an irreversible growth of the nucleus. The size of the critical nucleus is dependent on the supersaturation (smaller nucleus size at higher supersaturation), and thus on the overpotential.

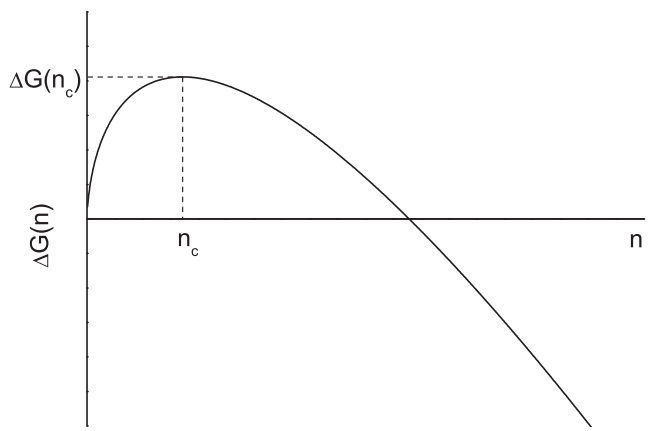

Figure 1.3: Nucleation work as a function of the nucleus size according to the classical (continuum) nucleation theory [14].

Equation 1.17 forms the basis for the thermodynamics of nucleation. However, it does not say anything about the rate, at which the nuclei appear at the electrode surface. The classical treatment of the nucleation has been developed by Becker and Döring [18]. The equation for the stationary nucleation rate is:

$$J_{st} = N_0 \Gamma \omega \exp\left(-\frac{\triangle G}{kT}\right). \tag{1.18}$$

Here J_{st} is the stationary nucleation rate, N_0 is the total number of potential nucleation sites, Γ is the non-equilibrium Zeldovich factor, which accounts for the deviation of the nucleation rate from quasi equilibrium [14], and ω is the rate of attachment of single atoms to the critical nucleus.

After nucleation, the crystallites of the new phase begin to grow. If one considers growth of single faces of the crystallites, one can distinguish two mechanisms of growth: direct attachment, in which the ions are reduced at the growth sites (kinks or steps) directly, and surface diffusion, where ions are reduced everywhere on the surface, become adatoms, and move towards the growth sites via diffusion.

In general one distinguishes three deposition modes of a metal onto a substrate of a different material, depending on the relationship between the free energy of the substrate σ_s and the sum of the free energies of the deposit σ_d and the interface between the deposit and the substrate σ_i. Additionally, the misfit between the lattice parameters of the substrate and the deposited metal that gives rise to strain in the deposit plays a role. Thus, if the relationship[1] $\sigma_i + \sigma_d < \sigma_s$ holds and the crystallographic misfit between the substrate and the deposit is negligible, then Frank-van der Merwe (or layer-by-layer) growth takes place, see Fig. 1.4a. If the crystallographic misfit is significant, then initially one or several monolayers of the metal are deposited. These layers are significantly strained. Formation and growth of unstrained 3D crystallites on top of the strained layer becomes energetically favorable. This mode is called Stranski-Krastanov growth mode, see Fig. 1.4b. Finally, if the condition $\sigma_i + \sigma_d > \sigma_s$ is satisfied, then Volmer-Weber growth mode, or 3D island formation mode takes place, see Fig. 1.4c. During electrodeposition, if Frank-van der Merwe or Stranski-Krastanov growth modes are favored, than the initial layer is usually (but not necessarily) deposited in the underpotential deposition regime, see Section 1.2.3.

Figure 1.4: Different deposition modes of a metal on a foreign substrate. a) Frank-van der Merwe growth, or layer-by-layer growth. b) Stranski-Krastanov growth mode, resulting in 3D island formation on top of predeposited metal overlayers (one atom to several atoms thick). c) Volmer-Weber growth mode, or 3D island formation mode.

The rate of growth of crystallites, as well as its dependence on time, potential, concentration etc., depends on the rate-determining mechanism for the ions to arrive from the bulk of the solution and to reduce to become metal ions. Thus, for the case of diffusion-controlled growth of a hemispherical cluster, the electrochemical current, and thus the growth rate, is given by Eq. 1.13. If the diffusion is not a problem and the metal adatom supply is limited only by the charge-transfer kinetics, then the electrochemical growth current of a hemispherical cluster is given by:

$$I(t) = \frac{2\pi V_m^2 i_0^3}{(zF)^2} \left(\exp\left[\frac{\alpha z F \eta}{RT}\right] - \exp\left[\frac{(1-\alpha) z F \eta}{RT}\right] \right)^3 t^2. \tag{1.19}$$

The case of mixed diffusion and charge-transfer limitation will be discussed in Chapter 7.

[1] This and the opposite conditions are called the Bauer criterion [17].

When the crystallites grow, the so-called diffusion zones develop around them. These are the regions around the crystallites, in which the concentration of the metal ions is reduced by diffusion to the crystallites, thus reducing also the supersaturation[1]. Thus, nucleation of new crystallites in these zones is inhibited.

In a real experiment, one cannot easily distinguish and study all the phases of nucleation and growth independently, especially not by conventional electrochemical techniques. That is why several theories have been developed to account for all these processes under different assumptions. In the following, we will present a theory developed by Scharifker and Hills (SH) [19], which accounts for multiple random nucleation on an electrode with subsequent growth and overlap of the 3D diffusion zones around the nuclei. In this model, the deposition is assumed to be diffusion-controlled. The model provides analytical expressions for the current vs. time dependence for two limiting cases of nucleation: instantaneous nucleation and progressive nucleation. Instantaneous nucleation assumes that a fixed number of nuclei N is formed in the very initial stage of deposition, and progressive nucleation assumes that the nuclei are formed during the whole experiment (until the whole electrode surface is covered by diffusion zones) with a rate $J_{st} = N_0 A$, where N_0 is the total number of nucleation sites and A is the nucleation rate per site. By fitting experimentally obtained chronoamperometry curves by the model, one can obtain various parameters such as the nucleation rate or the nucleus density.

As a starting point of the SH model we assume that a diffusion zone around a nucleus develops in such a way that its radius $\delta(t)$ is described as a function of time by the following relation:

$$\delta(t) = (kDt)^{1/2}, \tag{1.20}$$

where k is a numerical constant, determined by the conditions of the experiment. Further, it is assumed that at intermediate deposition times, the diffusion zones around nuclei grow and overlap, preventing flux of material to the nuclei from the sides of the diffusion zones. In this situation one can express the flux of material towards a nucleus as linear diffusion towards the circular area $S(t) = \pi kDt$ of a diffusion zone. Subsequently, the actual surface area of the electrode is calculated by the application of the Avrami theorem and the total flux is taken to be linear towards this area. Finally, the constant k is determined by comparing the resulting equation with Eq. 1.13 at very short time, since the nuclei can be considered as completely independent at this stage. In the case of instantaneous nucleation of N nuclei one obtains the following equation for the current density:

$$i(t) = \frac{zFC_b D^{1/2}}{(\pi t)^{1/2}} \left(1 - \exp\left[-N(2\pi)^{3/2}(C_b V_m)^{1/2} Dt\right]\right). \tag{1.21}$$

[1] Please note that these zones develop due to diffusion on the surface as well as diffusion in the electrolyte.

For progressive nucleation, the current density is given by:

$$i(t) = \frac{zFC_bD^{1/2}}{(\pi t)^{1/2}}\left(1-\exp\left[-\frac{2}{3}N_0A(2\pi)^{3/2}(C_bV_m)^{1/2}Dt^2\right]\right). \quad (1.22)$$

By setting the first derivatives of Eqs. 1.21 and 1.22 to zero, one can derive the current i_m and the time t_m, corresponding to the current maximum. A common way of comparing experimental data with the SH model is by plotting the dimensionless coordinates i^2/i_m^2 vs t/t_m. Equations 1.21 and 1.22 in these coordinates are given by:

$$\frac{i^2}{i_m^2} = \frac{1.9542}{t/t_m}\left(1-\exp\left[-1.2564(t/t_m)\right]\right)^2 \quad \text{instantaneous nucleation}, \quad (1.23)$$

$$\frac{i^2}{i_m^2} = \frac{1.2254}{t/t_m}\left(1-\exp\left[-2.3367(t/t_m)^2\right]\right)^2 \quad \text{progressive nucleation}. \quad (1.24)$$

Scharifker and Mostany (SM) have extended this model for a more general nucleation law [20]:

$$J(t) = AN_0\exp(-At). \quad (1.25)$$

They have also taken a somewhat different approach for the derivation of the current vs time relationship, initially defining the constant k by equating fluxes towards a hemispherical cluster and a circular projection of a diffusion zone on the surface. The current-time dependence of the SM model is given by:

$$i(t) = \frac{zFC_bD^{1/2}}{(\pi t)^{1/2}}\left(1-\exp\left[-N_0(2\pi)^{3/2}(C_bV_m)^{1/2}D\left(t-\frac{1-e^{-At}}{A}\right)\right]\right). \quad (1.26)$$

1.2.2.4 Shape of 3D crystallites on a foreign substrate

The equilibrium shape of a crystallite corresponds to a minimum of the total surface free energy for a given crystallite volume. For a crystallite, supported on a substrate, the total surface free energy F is defined as [14]:

$$F = \sum_j \sigma_j S_j + (\sigma_i - \sigma_s)S_i, \quad (1.27)$$

where σ_j and S_j are the specific surface free energies and the surface areas of the crystal faces in contact with the solution, σ_i and S_i are the specific interface free energy and the surface area of the crystallite-substrate interface, and σ_s is the specific free energy of the substrate[1]. In the case of the crystallites in an electrochemical environment, the surface free energy of a crystal face corresponds to the free energy of the interface between the crystal face and the electrolyte. In general, this free energy is different from the free energy of the same crystal face in vacuum.

[1] The word "specific" is dropped in the further discussion.

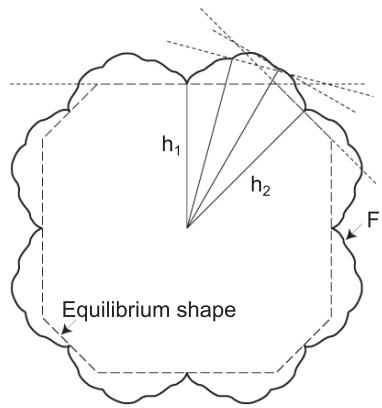

Figure 1.5: Cross section of the 3D surface free energy plot (solid line). The Wulff construction is used to determine the equilibrium shape of the crystallite (long dash). Please note that in the present image the surface free energy plot has cusps in the points where the plot touches the crystallite shape. This situation is only possible at $T = 0\,K$. At non-zero temperatures, these cusps are rounded, leading to the presence of the higher-index crystallographic planes in the equilibrium shape. The image is according to [21].

The equilibrium shape of an unsupported 3D crystallite can be constructed from the plot of the surface free energy in spherical coordinates by applying the well-known Wulff construction [21, 22]. As an example, Fig. 1.5 shows the cross section of the 3D surface free energy plot. To every point of the plot, a line is drawn from the origin W (Wulff point). Perpendicular to this line at its intersection with the spherical plot (or the polar plot in the cross section as in Fig. 1.5), a line is drawn. When all the latter lines are combined, the interior contour has the shape, which minimizes the total free energy of the crystallite for a fixed total island volume. This graphical construction is equivalent to applying the Legendre transform to the spherical free energy plot.

A popular method to determine the ratios between the surface free energies that correspond to crystal faces of different orientations is to apply the inverse Wulff construction to the images of the crystallites. One defines the Wulff point as the center of mass of a crystallite, and then applies the Wulff construction in reverse order to obtain the step free energy plot to within a constant sale factor. This method results in the following set of equations for different crystal faces j:

$$\frac{\sigma_j}{h_j} = K, \tag{1.28}$$

which states that the surface free energy of a crystal face is proportional to the shortest distance from the face to the center of the equilibrium shape (the so-called Wulff point) h_j, with the proportionality constant K being the same for different faces. Kaischew has

generalized the Wulff rule for the crystallites that are supported on a foreign substrate by defining the following relation for the substrate-crystallite interface (in addition to Eq. 1.28) [8]:

$$\frac{\sigma_k - \beta}{h^*_k} = K. \tag{1.29}$$

Here β is the so-called adhesion free energy, which is defined as $\beta = \sigma_k + \sigma_s - \sigma_i$, where σ_k is the free energy of crystallite face in contact with the solution; h^*_k is the shortest distance from the Wulff point to the interface.

In general, the shape of a crystallite during growth differs from that of the equilibrium shape. The growth shape is determined by the growth rates of the various facets rather than by their free energies. It is possible to derive an analogue of the Wulff rule valid for the shape of the growing crystal [15].

1.2.3 Metal underpotential deposition

Underpotential deposition (UPD) is a self-terminating electrochemical deposition process that occurs at potentials positive[1] of the reversible Nernst potentials in an electrolyte that contains ions of a different material than the material of the electrode. UPD results in the formation of a thin deposit, which can be between a submonolayer amount and a small number of monolayers, depending on the details of the system [23]. UPD is mostly observed in systems containing a metal electrode and a solution with ions of a different metal, however UPD on semiconductor surfaces [24] and UPD of non-metals [25] has also been reported. UPD processes attracted a lot of attention since they form model systems for studying adatom-adatom, adatom-substrate, and adatom-solution interactions.

In general, underpotential deposition occurs if the Bauer criterion $\sigma_s > \sigma_{i,s/m} + \sigma_{UPD}$ is satisfied, where $\sigma_{i\,s/m}$ is the free energy of the interface between the M layer and the substrate and σ_{UPD} is the free energy of the interface between the metal UPD layer and the solution. In the electrochemical literature the reason for the formation of a UPD layer is sometimes attributed to the stronger interaction energy between the substrate S and the metal to be deposited M than the M-M interaction energy, see e.g. [8]. It has been shown however that this is not always the case, as the anions that are usually present in the electrolyte can also affect the UPD. Since the adsorption of the anions changes the surface free energy of the electrode, it would be more correct to write the condition of the UPD layer formation in the presence of anions in the form of the Bauer criterion[2] $\sigma_s > \sigma_{i\,s/m} + \sigma_{i\,m/a} + \sigma^*_{UPD}$, where $\sigma_{i\,m/a}$ is the free energy of the interface between the M layer and the layer of co-adsorbed anions and σ^*_{UPD} is the free energy of the

[1] We assume the deposition of positive ions, such as Cu^{2+}.

[2] Please note that this criterion is true if the M atoms and the co-adsorbed anions form a bi-layer. However, in some systems a mixed monolayer is formed, for which this criterion has to be modified.

interface between the anion adlayer on the UPD layer and the solution. Thus, the anions can not only influence the structure of the UPD layer, but they can also promote UPD in systems where otherwise UPD would be impossible. For example, for the Cu deposition on Au(111) it has been found that the UPD is energetically unfavorable. However, due to the presence of the anions in the solution and their co-adsorption during the UPD, the process becomes energetically favorable and is observed experimentally [26].

1.3 Electrochemical techniques

The electrochemical experiments, presented in this thesis, were performed under potential control. For that a three-electrode cell was used. A three electrode cell consists of a working electrode (WE), i.e. the electrode of interest, a reference electrode (RE), which has a constant potential in a given solution and is used to measure the relative potential of the WE, and a counter electrode (CE), which supplies the current for the electrochemical reactions as well as double-layer charging to take place at the WE. The electrodes are connected to a device called potentiostat, which allows one to control the potential of the WE and measure the current flowing through the WE. We will describe two measurement techniques that can be carried out with a potentiostat.

1.3.1 Cyclic voltammetry

In cyclic voltammetry, the potential of the WE is varied linearly in time in a certain potential interval in a cyclic manner. During this variation of the potential, the electrochemical current through the WE is measured. In this experiment, it is customary to record the current as a function of potential, resulting in plots called cyclic voltammograms (CVs). There are two contributions to the current in a CV due to the non-Faradaic and Faradaic processes. The non-Faradaic processes do not result in the electrochemical reactions at the WE and only lead to the (re)charging of the double-layer. In a simple approximation, the double-layer can be represented as a parallel plate capacitor with a capacitance C_d. Thus, the charging current during a potential sweep can be represented as follows:

$$I_{ch} = C_d \omega, \tag{1.30}$$

where ω represents the potential sweep rate in $\mathrm{V\,s^{-1}}$.

The Faradaic processes are reactions that occur at the electrode surface and result in a charge transfer across the electric double-layer. Some examples of the Faradaic processes are metal deposition and ion adsorption. Please note that in a CV positive currents correspond to oxidation reactions (i. e. the electrode surface is accepting electrons) and negative currents correspond to reduction reactions (the surface is providing electrons).

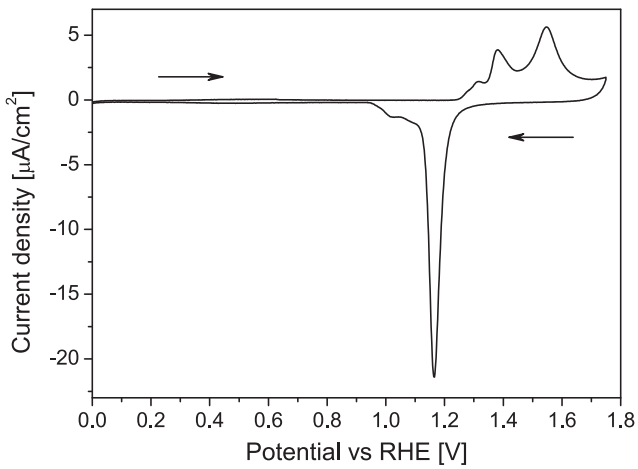

Figure 1.6: Cyclic voltammogram of Au(111) electrode in a 0.1 M $HClO_4$ solution. The scan rate is 5 mV s^{-1}. The image is reproduced with permission of [27].

As an example, figure 1.6 shows a CV of a Au(111) single crystal electrode in a 0.1 M $HClO_4$ solution. The positive peaks at 1.31 V, 1.38 V, and 1.55 V correspond to different stages of the formation of a gold surface oxide layer [28, 29]. The negative peak at 1.17 V is due to the reduction of the Au oxide layer. It has been shown that the peaks at 1.31 V and 1.38 V do not result in morphological changes of the Au(111) surface, whereas the oxidation peak at 1.55 V leads to the formation of a stressed oxide layer, which, upon reduction, leads to the formation of monatomic deep holes as well as monatomic high islands on the surface [30]. In the potential region between 0 V and 1.25 V (almost) no Faradaic processes take place. This potential region is called the double-layer region, as the potential change in this region results only in the double-layer (re)charging.

1.3.2 Chronoamperometry

Chronoamperometry (CA) is an electrochemical technique that is suited for the study of the kinetics of reactions, occurring at the WE. In this technique, the potential of the WE is changed in a stepwise manner and the current response of the system is measured as a function of time. Usually, the potential is stepped from a value, where the reaction of interest does not take place, to a potential, at which the reaction occurs. Again, both Faradaic and non-Faradaic processes may contribute to the current response of a system. The density of the non-Faradaic current that flows due to the (re)charge of the

double-layer is given by the following relationship:

$$I_{ch}(t) = \frac{\triangle E}{R} \exp\left(\frac{-t}{RC_d}\right), \tag{1.31}$$

where $\triangle E$ is the amplitude of the potential step and R is the electrolyte resistance. A typical time constant of the current variation due to the double-layer charging is $RC_d \sim 10\ ms$. After this time, the current flows mainly due to the Faradaic processes. A detailed analysis of the current evolution with time for different potential steps can yield kinetic insights into these processes.

Figure 1.7 shows and example of a CA curve corresponding to Cu UPD layer stripping from a Au(111) surface. The non-uniform time dependence of the current vs. time contains information about the kinetics of the layer dissolution. It can be analyzed using the SH model modified for the case of 2D nucleation and growth of vacancy islands in the Cu UPD layer [31].

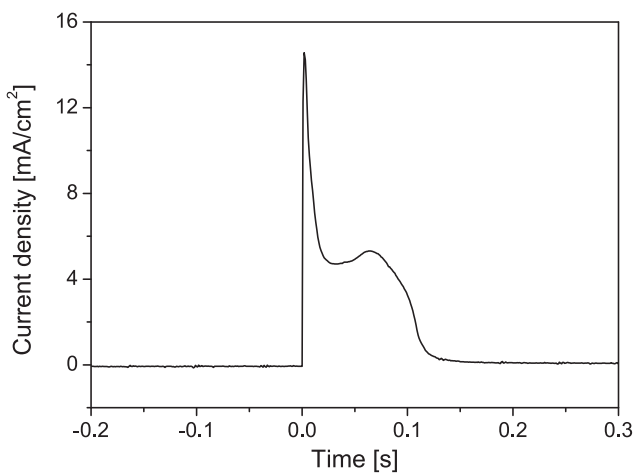

Figure 1.7: Chronoamperometry measurement of Cu UPD layer stripping from Au(111). The solution consists of 0.1 M H_2SO_4, 1 mM HCl, and 10 mM $CuSO_4$. The potential was stepped from 100 mV to 400 mV vs a Cu/Cu^{2+} quasi-reference electrode.

CA is especially suitable for studying electrochemical deposition processes, as the deposition at constant overpotential corresponds to constant supersaturation at the electrode surface[1].

[1] This is true if the concentration of the ions at the electrode is kept constant.

1.4 Vibrational spectroscopy

The spectroscopic techniques, Fourier transform infrared spectroscopy and surface enhanced Raman spectroscopy, described in this section, are based on probing molecular vibrations of the molecules adsorbed on a surface. Both techniques are based on the fact that molecules possess discrete levels of vibrational energy corresponding to different vibrational modes of the atoms. If a molecule is hit by a photon that has the same energy as the separation between two levels, the photon might be adsorbed. On the other hand, a molecule in an excited state may relax into a lower state by emitting a photon with the characteristic energy. Molecular vibration levels are found in the energy range that correspond to infra-red light. Thus, by studying the response of a sample to infrared radiation (either by studying adsorption or emission), one can identify molecules present at the electrode surface.

1.4.1 Fourier transform infrared spectroscopy

Fourier transform infrared spectroscopy (FTIR) is based on the adsorption of photons with the same energy as the energy gap between two vibrational levels of a molecule. In order to be able to adsorb a photon, the transition has to produce a change in the dipole moment. Thus, FTIR is sensitive towards polar bonds.

In a typical FTIR experiment, infrared light from a broadband source is shone onto an electrode and the intensity of the reflected light is analyzed. In this geometry one is sensitive only to the vibration modes of adsorbed molecules that are perpendicular to the surface. The modes that are parallel to the surface induce image dipoles in the electrode that are oriented in the opposite direction. Thus, the molecular dipole and the image dipole cancel each other, making such modes "invisible" with FTIR.

The "Fourier transform" in the FTIR stands for the method, with which the spectra are acquired. Instead of measuring the light intensity in a narrow range of wavelengths at a time, data is simultaneously collected in a wide spectral range. This raw data is then Fourier transformed to provide the actual spectrum.

1.4.2 Surface enhanced Raman spectroscopy

In surface enhanced Raman spectroscopy (SERS), monochromatic light of higher energy than the vibrational energy (visible light) is shone on the molecules. Most of this light is scattered elastically by the molecules, i.e. without the change of the photon energy (Rayleigh scattering). However, some of the light will scatter inelastically, resulting in photons of a different energy than the incident light (Stokes scattering). This energy is dependent on the vibrational modes of the bonds in the molecules. This process is the Raman effect. The Raman effect will produce light with discrete energy differences

relative to the energy of the incident light, which correspond to quanta of the vibrational normal modes of the molecule.

Since the probability of inelastic scattering is very small, the intensity of the Raman signal is weak and difficult to measure. To amplify the Raman signal, surface enhanced Raman scattering is employed, which provides an increase of the intensity by a factor of $\sim 10^6$. The surface enhancement occurs due to two effects: electromagnetic and chemical. The electromagnetic enhancement effect arises due to excitation of plasmons perpendicular to the surface by the incident light. Electrochemically roughened surfaces provide a lot of spots on the surface, where such plasmons can be excited and coupled to the molecules adsorbed on the surface. The chemical effect involves charge transfer between the chemisorbed species and the metal surface.

In principle, a similar selection rule for the vibrational modes parallel and perpendicular to the surface, as in the case of FTIR, can be applied to SERS. However, since the substrates that are used for SERS are roughened, the same molecular dipole may be parallel to some parts of the surface, but not parallel to the other parts. Thus, several image dipoles can contribute to the resulting scattered light intensity, removing (or at least weakening) this selection rule [32]. Additional selection rules might be also active, which are dependent on the nature of the surface enhancement mechanism [33].

In general, SERS has a lower sensitivity than FTIR. However, it provides several advantages. Firstly, SERS is more sensitive to backbone structures and symmetric bonds, which are (almost) not detectable with FTIR. Secondly, excitation in SERS is done in the visible light range, which simplifies the geometry of the electrochemical cell and allows accessing vibration levels at wavenumbers below 900 cm^{-1}. Accessing this wavenumber range with FTIR is very difficult as most of the materials that can be used for optical windows adsorb in this range. This wavenumber range is especially interesting, as the metal-adsorbate vibration frequencies (metal-chloride, metal-sulfur, etc.) are found in this range. Thus, FTIR and SERS can be viewed as complementary techniques that provide additional information about the vibrational structure of adsorbed molecules than can be obtained by using either alone.

1.5 Scanning tunneling microscopy

Since its invention by Binnig and Rohrer in 1981 [34], scanning tunneling microscopy (STM) has been the technique of choice for direct imaging of conducting surfaces at various conditions, as it provides superb spatial resolution. Also, STM measurements can be conducted in various environments, such as in vacuum, air, gas, and liquid.

In an STM experiment, a sharp metallic tip and a conducting surface are brought to within a distance of a few Ångströms from each other. A bias voltage, applied between the tip and the sample causes a current to flow. This current, which also flows in the

absence of a direct contact between the sample and the tip, arises due to a quantum-mechanical effect called tunneling. The imaging of the surface[1] is done by scanning the tip along the surface while keeping the tunneling current constant by performing feedback on it. The required adjustment in the tip-surface separation, to keep the tunneling current constant, reflects the height variations due to the morphology and the electronic states of the surface. The variations of the tip-sample separation as well as the longitudinal motion are accomplished by means of sensitive piezo-electric materials. Since the tunneling current depends exponentially on the distance between the tip and the surface, very high height resolution of the sample can be achieved. This makes STM capable of resolving single atoms on surfaces.

1.5.1 STM in electrochemical environment

During the use of STM in an electrochemical environment both the tip and the sample have to be immersed into an electrolyte. Since both the tip and the sample are conducting, they act as electrodes. In general, one would like to control the electrochemical potential of the tip and the sample independently, such that one could trigger reactions of interest on the sample and exclude unwanted reactions on the tip by choosing a proper potential. Reactions that take place at the tip could lead to changes of its shape, making the tip less sharp and unstable, and, in addition, could also result in electrochemical currents that are much larger than the tunneling current making the imaging of the surface impossible. To achieve independent potential control of the tip and the sample, a reference electrode and a counter electrode are added to the system and all electrodes are connected to a bi-potentiostat. The bi-potentiostat operates as a conventional potentiostat, but allows one to control the potentials of two electrodes, that is of the tip and the sample, independently, see Fig. 1.8.

However, in most of the electrochemical systems, connecting an STM to a bi-potentiostat is not enough to obtain a tunneling current clean of noise and interference. The reason for that is the relatively large surface area of the tip that is in contact with the electrolyte. In many electrochemical systems and for most tip materials, it is impossible to find a potential, where absolutely no Faradaic processes occur at the tip. These processes would lead to an electrochemical current flowing through the tip. This current is proportional to the surface area of the tip that is in contact with the solution. But also if such a potential could be found for a particular system, a double-layer would form at the tip/electrolyte interface. The total capacitance of the double-layer is also proportional to the contact surface area of the tip and the electrolyte. The electrolyte is a conductor that can also act as an antenna. Thus, a large double-layer capacitance

[1] This measurement mode is called the constant current mode. This mode has been used in the measurements, presented in the thesis.

would result in a better coupling for the low frequency signals (50 Hz) from the electrolyte to the tip. Also, slight variations in the capacitance of the double-layer would lead to large charging currents. Moreover, the high double-layer capacitance at the tip can greatly increase the high frequency noise of the sensitive tunneling current amplifier due to an increase of the capacitance at its input. Thus, it is necessary to isolate most of the surface area of the tip, leaving only the very apex exposed. This is generally accomplished by various tip coating procedures using different coating materials, such as polyethylene, Appiezon wax, electrophoretic paint, and even nail polish [35]. A description of the tip coating that we used can be found in Appendix A.

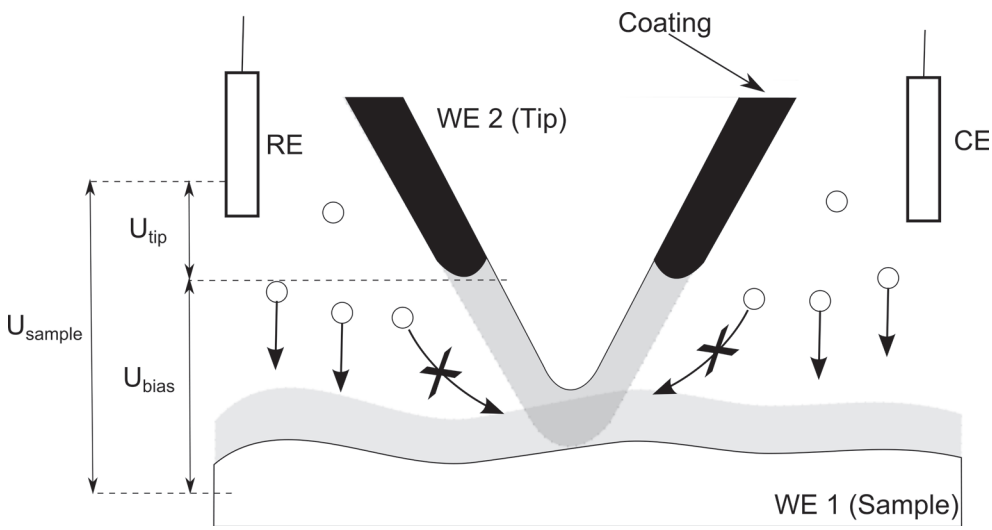

Figure 1.8: A schematic image of the electrochemical STM. Potentials between the tip and the reference electrode (U_{tip}) and the sample and the reference electrode (U_{sample}) are controlled independently via a bi-potentiostat. Except for its apex, the tip is coated with an insulating film in order to minimize Faradaic currents and capacitive coupling to the solution. Double-layers around the tip and the sample are represented by the gray areas. In the vicinity of the area, where tunneling occurs, double-layers may overlap. Also, the lateral extent of the tip may inhibit diffusion of ions towards the area being imaged. WE, RE, and CE represent the working electrode, the reference electrode, and the counter electrode respectively.

In general, STM is considered a non-intrusive technique that does not influence the surface being imaged. However, in an electrochemical environment the influence of the STM tip on the surface underneath it could be substantial. Two different mechanisms of the possible tip influence are shown in Fig. 1.8. Although a good STM tip has an apex diameter of only a few nanometers, its shape is usually conical. This leads to a significant lateral extent of the tip in the vicinity of the sample surface that is imaged.

During an electrochemical reaction, where substantial mass transport is involved, the vicinity of the tip could impair diffusion of ions to/from the electrode surface. This is in particular true, as the tip is positioned at a close distance from the sample in order to get into tunneling regime. In liquid, this distance is somewhat larger than in vacuum, since the tunneling barrier is lower[1]. On the other hand, the typical width of the double-layer region around an electrode is of the same order of magnitude. Thus, the double-layers of the tip and the sample may overlap around the position where imaging is done, resulting in a local deviation of the electrochemical potential. These tip effects have to be taken into account when performing STM experiments in electrochemical environment.

[1] The tunneling barrier is typically 1 eV in liquid vs $\sim$ 5 eV in vacuum [36].